This article has been amended to include a factual correction. An error was identified subsequent to its original publication. This error was acknowledged on page 360, volume 34, issue 5. The online article and its erratum are considered the version of record.

ORIGINAL ARTICLE

The Relationship Between Mechanical Properties, Ultrastructural Changes, and Intrafibrillar Bond Formation in Corneal UVA/Riboflavin Cross-linking Treatment for Keratoconus

Shao-Hsuan Chang, MSE; Ashkan Eliasy, MEng; Kai-Jung Chen, MS; You-Ren Ji, MS; Tai-Horng Young, PhD; Tsung-Jen Wang, MD, PhD; Colin E. Willoughby, MD, FRCOphth; Kevin J. Hamill, PhD; Ahmed Elsheikh, PhD

ABSTRACT

PURPOSE: To determine the relationship between mechanical behavior in cross-linked corneas and changes in the corneal ultrastructure after corneal cross-linking (CXL).

METHODS: Porcine corneas were treated following the "Dresden" protocol, the current gold standard for clinical treatment, consisting of dropwise application of 0.1% riboflavin in 20% dextran followed by 30 minutes of ultraviolet-A (UVA) irradiation. The effect of CXL was assessed using uniaxial tensile testing, transmission electron microscopy, and Fourier transform infrared spectroscopy, with results compared against corneas treated with each of the treatment solution components individually.

RESULTS: UVA/riboflavin cross-linked corneas displayed 28% ± 17% increase in the material tangent modulus compared with dextran treatment alone, and altered collagen architecture within the first 300 μm of stromal depth consisting of 5% increase in the thickness of collagen fibrils, no significant changes to interfibrillar spacing, and an 8% to 12% decrease in number of fibrils per unit area. Fourier transform infrared spectroscopy confirmed formation of interfibrillar bonds (P = .012) induced by UVA-mediated CXL.

CONCLUSIONS: The data support a model wherein collagen fibril diameter and structural density are fundamental parameters in defining tissue stiffening following UVA/riboflavin CXL and provide benchmarks against which modifications to the Dresden CXL protocol can be evaluated.

[*J Refract Surg.* 2018;34(4):264-272.]

Keratoconus is a corneal thinning disease that results in a focally reduced corneal radius of curvature, abnormal wavefront aberrations, and a localized reduction in corneal thickness and stiffness. These aberrations lead to a decline in visual function that ultimately may require corneal transplantation.[1] Corneal cross-linking (CXL) with riboflavin and ultraviolet-A (UVA) is an established treatment for progressive keratoconus and currently is the only therapeutic approach that is capable of significantly altering disease progression.[2] Available for many years in Europe, this treatment option has been recently approved by the U.S. Food and Drug Administration for use in the United States.[2] The so-called "Dresden" or "standard" protocol is the current standard approach for CXL for keratoconus and consists of 30 minutes' exposure to 3 mW fluence (5.4 mJ/cm^2) following 30 minutes of soaking in 0.1% riboflavin.[3]

The Dresden protocol involves removal of the corneal epithelium followed by dosing of the corneal stroma with

From the School of Engineering, University of Liverpool, United Kingdom (S-HC, AEliasy, K-JC, AElsheikh); the Department of Eye and Vision Science, University of Liverpool, United Kingdom (CEW, KJH); St. Paul's Eye Unit, Royal Liverpool University Hospital, Liverpool, United Kingdom (CEW); Institute of Biomedical Engineering, College of Medicine and College of Engineering, National Taiwan University, Taipei, Taiwan (Y-RJ, T-HY); the Department of Ophthalmology, Taipei Medical University Hospital, Taipei, Taiwan (T-JW); the Department of Ophthalmology, School of Medicine, College of Medicine, Taipei Medical University, Taipei, Taiwan (T-JW); and NIHR Biomedical Research Centre for Ophthalmology, Moorfields Eye Hospital NHS Foundation Trust and UCL Institute of Ophthalmology, United Kingdom (AElsheikh).

Submitted: September 22, 2017; Accepted: January 10, 2018

© 2018 Chang, Eliasy, Chen, et al., licensee SLACK Incorporated. This is an Open Access article distributed under the terms of the Creative Commons Attribution 4.0 International (https://creativecommons.org/licenses/by/4.0). This license allows users to copy and distribute, to remix, transform, and build upon the article, for any purpose, even commercially, provided the author is attributed and is not represented as endorsing the use made of the work.

The authors thank Alison Beckett at Biomedical Electronic Microscopy Unit for teaching techniques and preparing materials, and Brendan Geraghty at Biomechanical Engineering Group in the University of Liverpool for help with mechanical settings.

Correspondence: Kevin J. Hamill, PhD, University of Liverpool, Eye and Vision Science, Room 285, The Apex Building, 6 West Derby Street, Liverpool, Merseyside L78TX, United Kingdom. E-mail: Kevin.Hamill@liverpool.ac.uk

doi:10.3928/1081597X-20180220-01

0.1% riboflavin in 20% dextran for 30 minutes, then exposure to ultraviolet light over a 30-minute period. The rationale behind this approach is that photo-polymerization, in the presence of the photosensitizer riboflavin, leads to creation of chemical bonds between substrates within the corneal stroma, including between collagens and proteoglycans and other stromal proteins.[3-5] The effects of these induced cross-links have been variously reported as increases in tissue stiffness, resistance to enzymatic digestion, changes to ultrastructure, and altered swelling behavior.[6-9] However, these studies have generally evaluated the overall effects of the full CXL protocol without separating the contribution of individual aspects of the treatment and there are some differences in outcomes reported.[5,6,10,11]

Mechanical properties of biological tissues are largely dependent on the intertwining of collagen fibrils, linked lamina layers, and interfibrillar spacing.[12-14] Therefore, the efficacy of the Dresden CXL protocol is believed to be dependent on changes to the mechanical properties of the tissue induced through modifying the characteristics of collagen fibrils within the cornea and the induction of intrafibrillar bonds, with the overall level of effect being dependent on treatment depth.[15,16] Previous studies have attempted to evaluate mechanical properties and the effective CXL penetration depth by specifically examining anterior and posterior corneal layers.[9,17,18] These studies demonstrated that the CXL effect is predominantly located within anterior stroma but did not specify the parameters that may be involved in determining and defining the amount of the tissue stiffening induced. Indeed, the relationship between the mechanical behavior of the cross-linked cornea and its ultrastructure is poorly explored, and the specific contribution of the dextran within the riboflavin solution has not been reported.[18,19]

Numerous modifications to the Dresden protocol are being tested in clinical settings; therefore, defined knowledge of the effect of the current treatment regimen is needed to provide a benchmark against which these modifications can be compared and moreover for rationale design of alternative approaches. The current study aimed to improve this understanding by systematically investigating the role of dextran and the effect of UVA/riboflavin CXL in inducing mechanical and ultrastructural changes in the porcine cornea.

MATERIALS AND METHODS

CXL Procedure and Experimental Design

Fresh porcine eyes were collected from an abattoir, washed with phosphate-buffered saline (PBS) (Sigma, Dorset, United Kingdom), the central corneas excised, and the corneal epithelium removed. To control for inter-animal variation, each cornea was cut into two segments in a superior-inferior fashion, with one being used as the test sample and the other for the control treatment (**Figure A**, available in the online version of this article).

There were four groups. The PBS vs PBS group (control) contained 6 corneas and each half cornea was topically treated with PBS in 3-minute intervals for 1 hour and used to examine the intrinsic differences between the two segments of each porcine cornea. The PBS vs riboflavin+PBS group contained 6 corneas and each corneal segment was topically treated in 3-minute intervals for 1 hour with either PBS or 0.1% riboflavin (Sigma) prepared in PBS. The PBS vs riboflavin+dextran group contained 6 corneas and treatment was the same as for the PBS vs riboflavin+PBS group, except that the riboflavin was prepared in 20% dextran (Sigma). The dextran vs riboflavin+dextran+UVA group contained 10 corneas and half were treated following the conventional Dresden protocol,[3] with the anterior surface of the corneas treated with 5 mL of 0.1% riboflavin in 20% dextran at 3-minute intervals for 30 minutes, followed by UVA (370 nm) illumination at 3 mW/cm^2 (Opto Xlink; Mehra Eyetech Pvt. Ltd., Delhi, India) for a further 30 minutes. Topical dosing of riboflavin with dextran drops was continued every 3 minutes during the UVA irradiation (for full CXL details following the standard convention, see **Table 1**).[20] CXL corneas were compared to fellow segments treated with 20% dextran only.

Following treatment, the corneal tissues were dissected for mechanical testing and for ultrastructural analysis (**Figure A**).

Tensile Testing

Corneal stiffness was examined using a uniaxial tensile tester (Instron 3366; Instron Engineering Corporation, Norwood, MA), equipped with a 10N load cell. Two strips (3 mm width × 6 mm length) cut in the superior-inferior direction at the central cornea were inserted vertically into custom-designed clamps and the protocol set to apply a maximum loading stress of 0.125 MPa, slightly above the stress expected under an intraocular pressure of 80 mm Hg.[21] A constant extension of 1 mm/min was applied and the corresponding stress (applied force divided by cross-sectional area) and strain (extension over original length) measured continuously. Five conditioning cycles,[21] with 4-minute recovery periods between two cycles, were performed. The tangent modulus (Et), the gradient of a tangent of the stress-strain behavior pattern, was calculated at different stress levels to derive the overall stiffness of the tissue.[22,23]

TABLE 1
CXL Methods

Parameter	Condition
Treatment target	Porcine
Fluence (total) (mJ/cm^2)	5.4
Soak time and interval (min)	30(q3)
Intensity (mW/cm^2)	3
Treatment time (min)	30
Epithelium status	Off
Chromophore	Riboflavin (Sigma, Dorset, United Kingdom)
Chromophore carrier	20% dextran
Osmolarity	Hypo-osmolar
Chromophore concentration	0.10%
Light source	Opto Xlink (Mehra Eyetech Pvt. Ltd., Delhi, India)
Irradiation mode (interval)	Continuous

CXL = corneal cross-linking

Transmission Electron Microscopy (TEM)

TEM was performed as described previously.[6] Briefly, the specimens were isolated from the central regions of cornea (**Figure A**) and fixed overnight with 2.5% glutaraldehyde (TAAB Laboratories Equipment Ltd., Reading, United Kingdom) in 0.1% tannic acid. Thereafter, specimens were dissected into 1 × 2 mm blocks and incubated with 4% osmium (TAAB), followed by serial dehydration through an acetone gradient (30%, 50%, 70%, 90%, and 100%) (Sigma). Specimens were then infiltrated and embedded in medium resin (TAAB) and ultrathin 70-nm thickness sections cut using a diamond knife microtome and collected onto 200 mesh copper grids (Ted Pella, Inc., Reading, CA). Sections were examined using a Tecnai G2 spirit BioTWIN Transmission electron microscope (FEI Company, Hillsboro, OR) operated at 120 kV and 60 k-fold magnification with a charge coupled device camera. Tissues were sampled at five depth intervals from the top of the anterior stroma: 0 to 50, 80 to 150, 200 to 250, 300 to 350, and 400 to 450 µm.

Collagen fibrils in longitudinal, frontal, and oblique profiles were observed in TEM images; only those in frontal profiles were used for quantitative analysis with analyses performed using Fiji software (National Institutes of Health, Bethesda, MD). Ultrastructural parameters evaluated were: mean diameter of collagen fibrils, interfibrillar spacing, and number of fibrils per unit area. For mean diameter of collagen fibrils, circular spots in frontal profiles were isolated and exported and diameters measured. The calculation of interfibrillar spacing was generated from **Equation 1** while assuming that the collagen fibrils were evenly distributed:

$$R + D = \sqrt{A/N} \quad (1)$$

Here R was defined as interfibrillar spacing (nm), D as mean diameter of collagen fibrils (nm), A as the area of selected zone of measurement (nm^2), and N as the number of fibrils (circular spots) within the selected zone. The number of fibrils per unit area was determined by randomly localizing a window of fixed unit size (300 × 300 nm) and the number of circular spots counted.

The distribution curve of collagen fibrils was assessed with a bespoke code using MATLAB 2016b software (The MathWorks, Inc., Natick, MA). Original images were converted to binary using adaptive thresholding and a custom-designed collagen fibril detection system, using the Circular Hough Transform–based algorithm,[24,25] was established to analyze the radius of circular objects in frontal profiles of TEM images. Distribution curves were generated by plotting the frequency in 2-nm increments against fibril radius.

Fourier Transform Infrared (FTIR) Absorption Spectroscopy

Fresh porcine corneas were treated with either PBS, 0.1% riboflavin in 20% dextran, or the full Dresden protocol (6 per group), lyophilized for 3 days, then measured with FTIR spectroscopy using a Nicolet 6700 FTIR spectrometer (Thermo Fisher Scientific, Chelmsford, MA) with an attenuated total reflection module. Sixty-four accumulative scans were taken with a resolution of 4 cm^{-1} between 800 and 4,000 cm^{-1}. Data were collected using OMNIC software (Thermo Fisher Scientific). Analyses of FTIR spectra of each condition were obtained with a combination of four spectral intervals (υ [C = O] absorption of amide I [1,680 to 1,630 cm^{-1}], δ (NH_2) absorptions of amide II [1,570 to 1,515 cm^{-1}], υ [C – N] absorptions of amide III [1,350 to 1,200 cm^{-1}), and υ [C – O] absorptions of carbohydrate moieties [1,150 to 1,000 cm^{-1}]). Area under the curve at each interval was analyzed using KnowItAll ID Expert software (Bio-Rad, Hercules, CA).

Statistical Analysis

Results for mechanical, ultrastructural, and FTIR spectra analyses are presented as mean ± standard deviation and statistical significance calculated using one-way analysis of variance with Turkey's HSD post-hoc tests. The Mann–Whitney *U* test (two-tailed) was used for analyzing the statistical difference of the dis-

tribution curves. *P* values of less than .05 were considered statistically significant.

RESULTS

UVA/riboflavin treatment and dextran-mediated dehydration both contribute to mechanical property changes in CXL. To isolate the effect of the individual components of UVA/riboflavin CXL, uniaxial tensile experiments and TEM were conducted on a set of porcine eyes split into paired comparison groups. To account for inter-animal variability, each cornea was cut in two and half treated with the treatment and compared against the control (**Figure A**) (tensile measurements and ultrastructural analyses were performed on the same cornea). Comparison groups were: PBS vs PBS, riboflavin+PBS vs PBS, riboflavin+dextran vs PBS and riboflavin+dextran+UVA vs dextran (**Figure A**).

The tangent modulus (Et) versus stress (σ) for each corneal strip was determined and the overall stiffening effect indicated by the ratio of the tangent modulus ($Et_{experimental}$ / $Et_{control}$). Comparisons concentrated on tangent modulus ratios at a stress of 0.03 MPa, which is equivalent to a physiological intraocular pressure of approximately 25 mm Hg.[21] As expected, no significant differences were observed where both corneal segments were treated identically with PBS, confirming the validity of our intra-eye control system ($Et_{experimental\ PBS}$ vs $Et_{control\ PBS}$: 1.36 ± 0.32 vs 1.43 ± 0.30 at 0.03 MPa, respectively, P = .075, **Figures BA-BB**, and **Table A**, available in the online version of this article). Riboflavin in PBS treatment also caused no stiffening (riboflavin in PBS: 1.45 ± 0.15 vs PBS: 1.38 ± 0.17, P = .448, **Figure BC**, **Table A**). However, the riboflavin+dextran group displayed a 13% ± 9% tangent modulus increase compared to their internal PBS control (riboflavin in dextran: 1.52 ± 0.17 vs PBS: 1.34 ± 0.18, P = .011, **Figure BD**, **Table A**). Comparing the effect of the full Dresden CXL protocol to the effect of dextran treatment alone, we observed a 28% ± 17% increase in tangent modulus in the corneal segments treated by the Dresden protocol (riboflavin+dextran+UVA: 2.09 ± 0.17 vs dextran: 1.62 ± 0.18, P < .001, **Figure BE**, **Table A**).

The differences observed with dextran alone were somewhat surprising, but on comparing the tissue thicknesses following treatments, we observed statistically significant reduced thicknesses in the dextran-treated samples compared with their PBS controls that were indicative of dehydration (mean thickness riboflavin in dextran: 0.79 ± 0.04 mm, PBS: 1.05 ± 0.39 mm, $P = 1.39 \times 10^{-6}$) (**Figure BF**, **Table A**). Correcting the tangent modulus readings with these thickness measurements removed the apparent dextran effects, whereas a residual stiffening effect was still observed in the samples treated with the Dresden protocol after correction (**Figure BG**). Together, these data demonstrate that dextran treatment alone causes dehydration and therefore an apparently increased stiffening, whereas corneas treated with UVA/riboflavin exhibit further increased stiffening beyond that caused by the dextran treatment alone.

UVA/Riboflavin Treatment Causes Depth-Dependent Changes to Collagen Fibril Ultrastructure

Next, we measured changes to the collagen ultrastructure of specimens, measured at five different depth intervals using TEM (**Figure C**, available in the online version of this article, and **Figure BA**; representative images at 80 to 150 mm) and the obtained images were used to determine collagen fibril diameter (**Figure BB**), interfibrillar spacing, and fibril number per unit area (density) (**Table B**, available in the online version of this article). The overall morphologies of the collagen ultrastructure did not change following PBS or riboflavin in PBS treatment in the absence of UVA (**Figure C**, **Table B**). However, the dextran treatment led to significantly thinner collagen fibrils (**Figure 1A**), as well as reduced interfibrillar spacing and denser packing at all depth intervals compared to its PBS control (**Figure C**). Because dextran also causes loss of tissue hydration, we used a mathematical method to correct for dehydration effects to identify the true structural changes.[26] The relationship between thickness (T) and hydration (H) was modelled using the equation: T = 0.2*e^(0.33*H), which has been shown to be effective for these types of calculation.[26] The reduction in thickness followed an exponential decrease in tissue hydration, which we used to calculate the hydration state of the tissues and therefore calculate swelling factors at each depth interval (**Table C**, available in the online version of this article). Analysis of fibril diameter at each depth interval revealed that although dextran treatment caused a reduction in the frequency of large collagen fibrils compared to PBS treatment (**Figure 1B**; 80 to 150 mm, **Tables B-C**) in the uncorrected data, when correction for swelling factors was included, no significant differences were detected (**Figure 1B**, **Figure D**, available in the online version of this article), indicating that dextran treatment alone has no effect on collagen fibril diameter.

In analyzing the effect of the Dresden UVA/riboflavin CXL protocol on corneal ultrastructure, both segments within our intra-eye comparisons were treated with dextran. Therefore, any residual difference between the internal controlled comparison groups reflected a true effect of the CXL procedure. Analysis revealed a small but statistically significant increase in collagen fibril diameter in the CXL group at 80 to 150 µm (5% ± 2%, P < .01) and 200 to 250 µm depths (6% ± 3%, P < .01), with no differences observed at any other depth intervals (**Figures 2C-2D**, **Figure D**). No statistical differences in

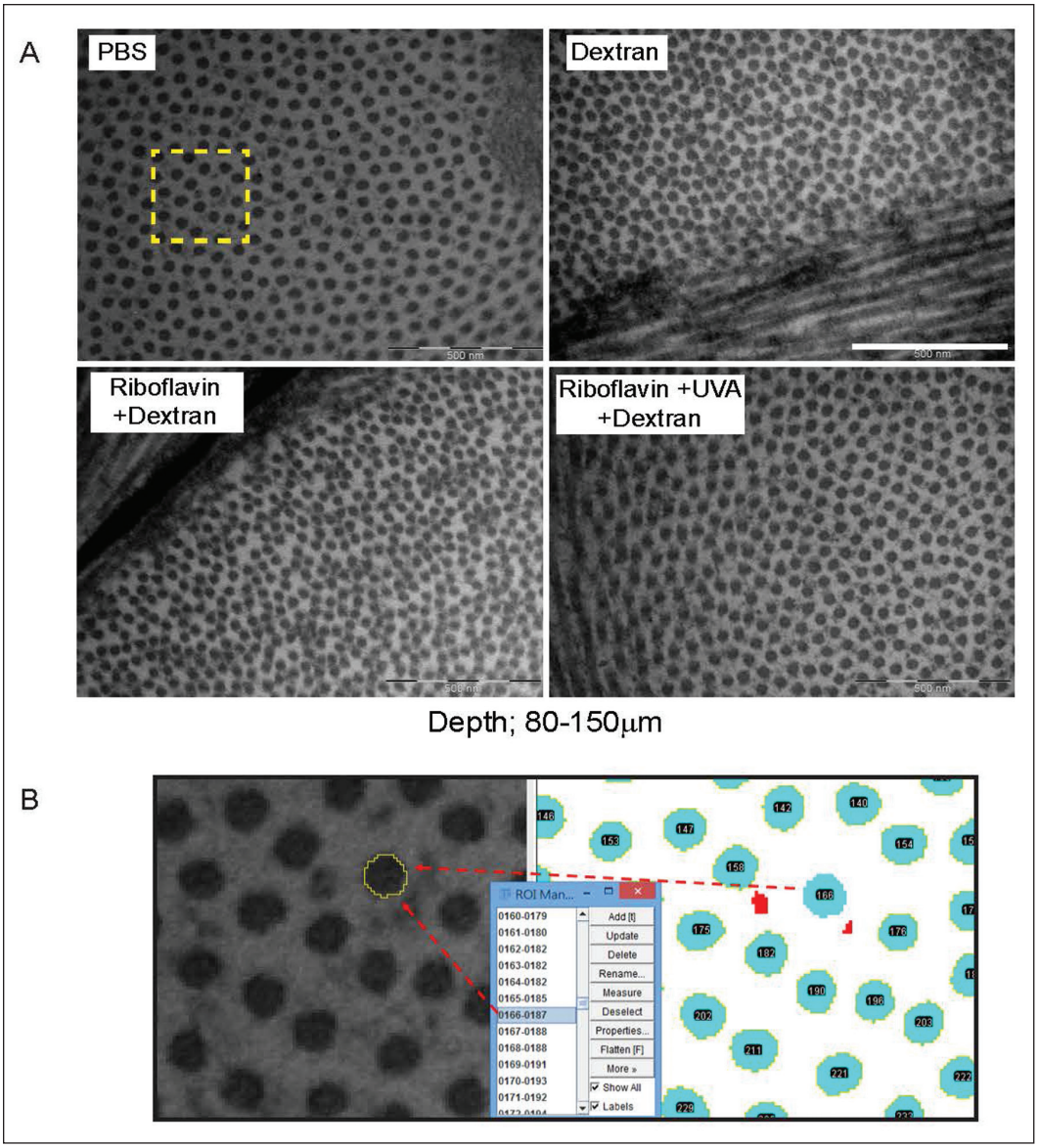

Figure 1. Transmission electron microscopy (TEM) images of porcine corneas imaged at a depth of 80 to 150 μm. (A) Representation TEM images of phosphate-buffered saline (PBS), riboflavin in dextran, and dextran only and riboflavin/dextran/ultraviolet-A (UVA) cross-linked corneas. Bar = 500 nm. (B) An area of 300 x 300 dpi (yellow dashed square) is shown at higher magnification with an example of the measurement of the area and density of collagen fibrils.

interfibrillar spacing between treatments were observed at any depths (**Figure 2E**), but the Dresden protocol caused a decrease in the number of fibrils per unit area in the anterior 250 µm of the tissue (0 to 50 µm: 6% ± 5%, $P < .05$; 80 to 150 µm: 11% ± 7%, $P < .01$; 200 to 250 µm: 11% ± 5%, $P < .01$) (**Figure 3**, **Table B**). Together, these data indicate that the UVA/riboflavin CXL procedure creates relatively small, depth-localized changes to the collagen ultrastructure.

Individual Ultrastructural Measurements Are Insufficient to Predict Mechanical Changes

Because we had performed the tangent modulus and ultrastructural measurements on the same eye (**Figure A**), we were able to directly compare the values obtained (**Figure 3**). Comparisons were made between mechanical outcomes measured at 0.03 MPa stress and structural parameters were determined from tissues in relaxed states. Collagen fibril diameter at 80 to 150 µm, intrafibril spacing increases, and collagen fibril density decreases each displayed correlation with tangent modulus increases across the test population (diameter: r^2 =0.23, **Figure 3A**; spacing: r^2 = 0.39, **Figure 3B**; density: r^2 = 0.52, **Figure 3C**). When percentage change on an individual eye basis was plotted, none of the individual ultrastructural parameters were independently indicative of the overall tissue stiffness (**Figure 3D**). However, when considered in combination, the ultrastructural measurements performed better, with a positive correlation of 0.177 (collagen fibril diameter + fibril density – interfibrillar spacing, **Figure 3E**).

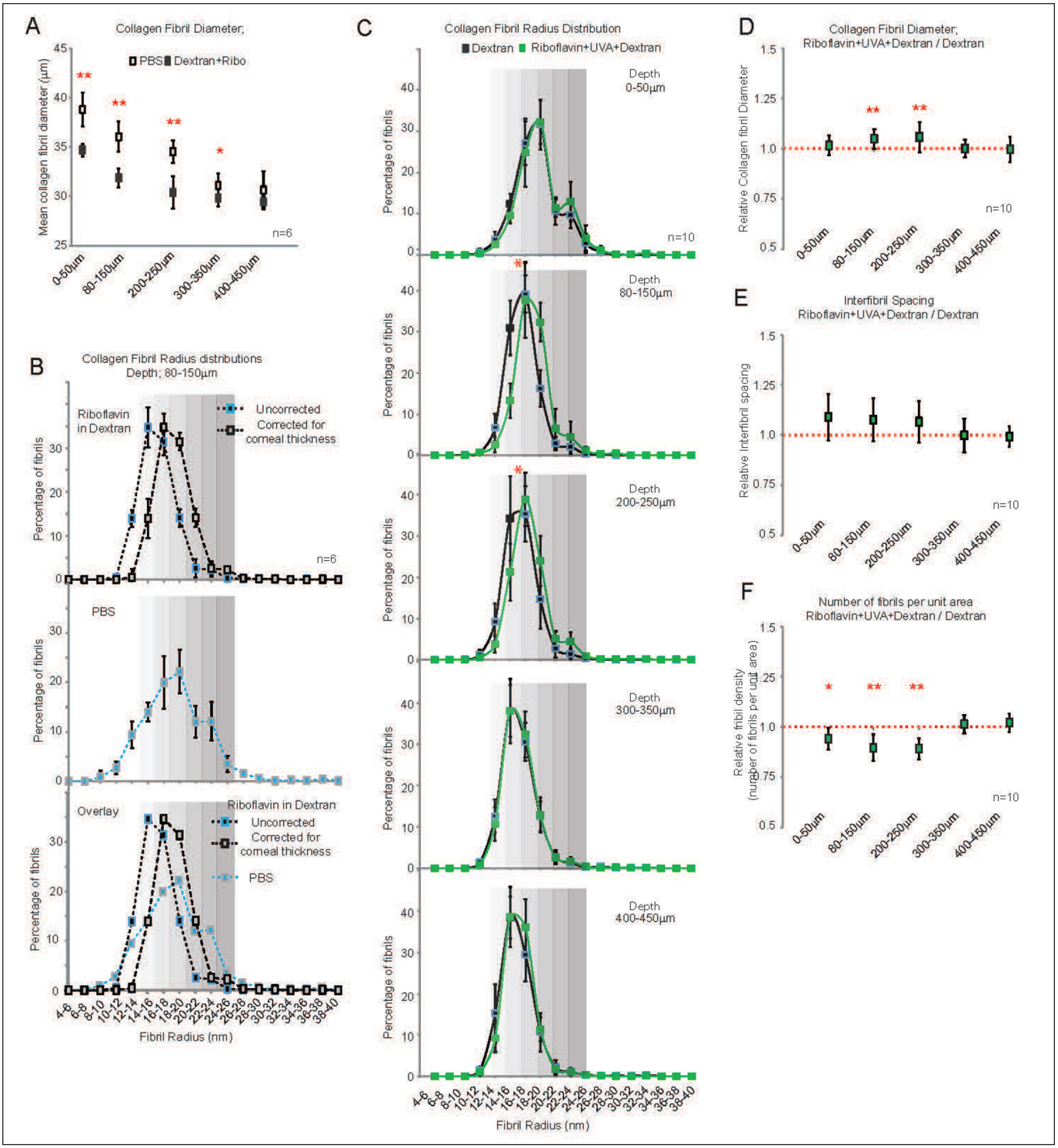

Figure 2. Measurement of ultrastructural parameters and collagen fibril distribution at different depth intervals. (A) Mean collagen fibril diameters of phosphate-buffered saline (PBS) and riboflavin in dextran at each depth interval. (B) Collagen fibril diameter distributions plotted as either uncorrected values from the riboflavin+dextran group (top panel, black filled squares) or corrected for dehydration (top panel, gray squares) or its corresponding PBS control (middle panel, blue filled squares). Traces are shown overlaid in bottom panels. Gray filled background added to aid visualization. (C) Collagen fibril diameter distribution curve of corneal cross-linking group (green boxes) and its dextran control (black boxes) at each depth interval. (D) Relative collagen fibril diameter. (E) Relative interfibrillar spacing. (F) Relative collagen density of the corneal cross-linking group relative to its dextran group at each depth interval. Values are plotted as mean ± standard deviation from n = 6 (A and B) or n = 10 (C, D, E, and F). Asterisks denote significant differences from control groups, with $*P < .05$ and $**P < .01$. UVA = ultraviolet-A

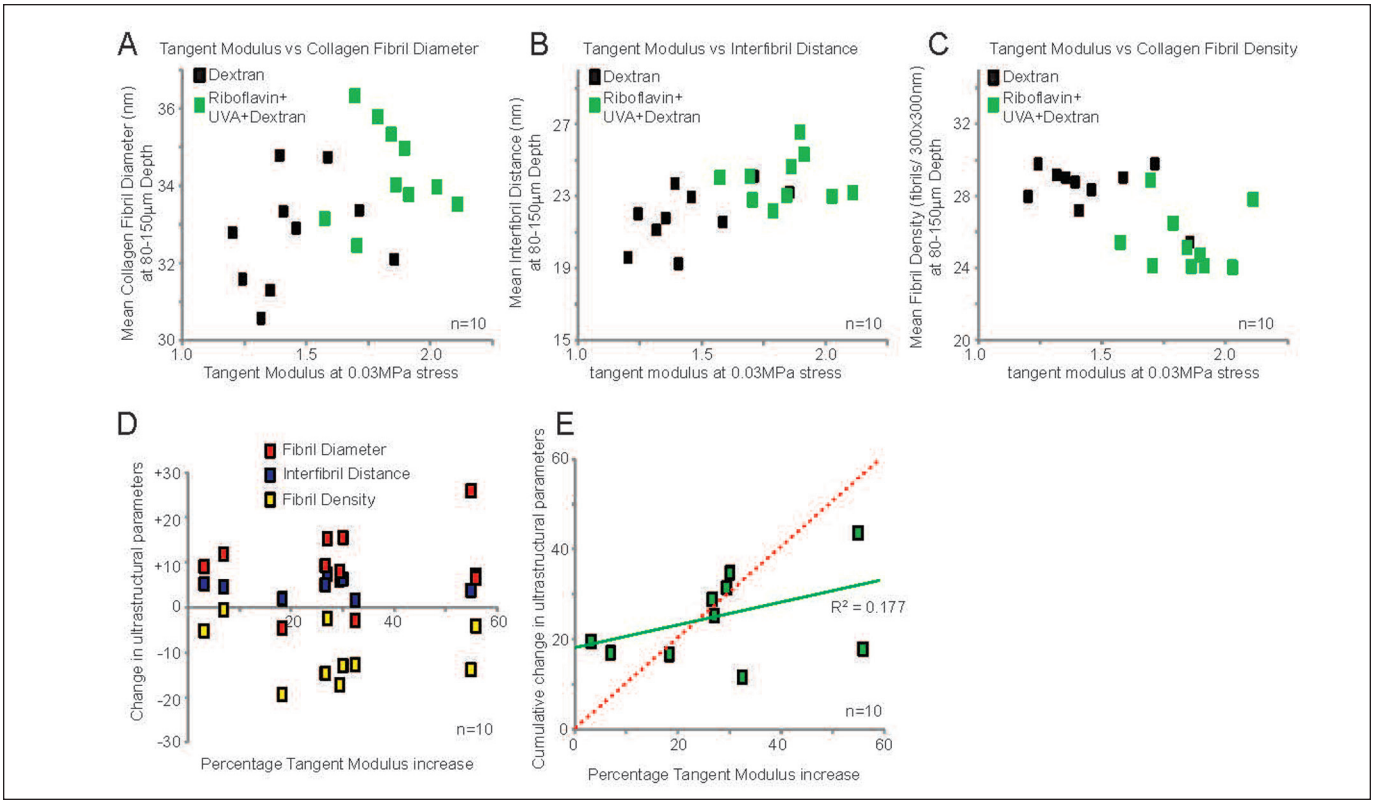

Figure 3. Correlation between ultrastructural parameters and tangent modulus. Tangent modulus at 0.03 MPa versus (A) collagen fibril diameter, (B) interfibrillar spacing, and (C) collagen fibril density. Black boxes = dextran-treated eyes; green boxes = riboflavin+ultraviolet-A (UVA)+dextran–treated eyes. (D) Percentage change in tangent modulus versus percentage change in each ultrastructural parameter. Each box represents the measurements from one eye for either fibril diameter (red), interfibril distance (orange), or fibril density (yellow). (E) Percentage change in tangent modulus plotted against the cumulative effects of percentage change in fibril diameter + interfibril spacing – fibril density. Each box represents one eye. Green line = linear line of best fit; red dotted line = 100% correlation

FTIR Spectroscopy Reveals the Formation of New Amide Bonds in CXL Corneas

To assess the detailed chemical reactions and the conversion of chemical bonds within the corneal tissue after UVA/riboflavin CXL, FTIR spectroscopy measurements were performed on corneas treated with either PBS, riboflavin+dextran, or riboflavin+dextran+UVA (**Figures 4A-4B**). The relevant characteristic bands were: amide I C = O stretching vibration (1,680 to 1,630 cm^{-1}), amide II NH_2 bending vibration (1,570 to 1,515 cm^{-1}), amide III C-N stretching vibration (1,350 to 1,200 cm^{-1}), and C-O bond stretching vibration (1,150 to 1,000 cm^{-1}). The area under each band was calculated, and the deformation vibrations of CH_2 (1,485 to 1,360 cm^{-1}) were used as an internal standard to determine the intensity ratios (**Figure 4C**, **Table D**, available in the online version of this article). These analyses revealed significant increases in the C-O stretch peak, decreased C-N stretch, and increased NH_2 deformation following CXL (**Figure 4C**). Plotting the ratio of C-N stretch to NH_2 deformation suggests that the decrease intensities of amide II infrared absorption bands are likely to be accompanied by an increase in the formation of amide III bonds (riboflavin+dextran+UVA = 2.5 ± 0.5; PBS = 1.7 ± 0.3; riboflavin+dextran = 1.8 ± 0.2; **Figure 4D**, **Table D**).

DISCUSSION

In this study, we have characterized how corneal mechanical properties relate to ultrastructural changes following the Dresden protocol treatment and identified the contribution of the different components of the protocol to observed effects. Specifically, our data demonstrate that the increases in corneal stiffness measured following Dresden protocol treatment arise from a combination of dextran-mediated dehydration and UVA/riboflavin–induced new bond formation and depth-dependent increases in collagen fibril diameter.

Tissue stiffness is considered a combination of the internal geometry of the tissue and the properties of the material itself. Therefore, although our data indicate that almost half of the measured stiffening effect of the Dresden protocol as measured ex vivo comes from the dextran component of the protocol, these effects can be explained by dehydration effects. How-

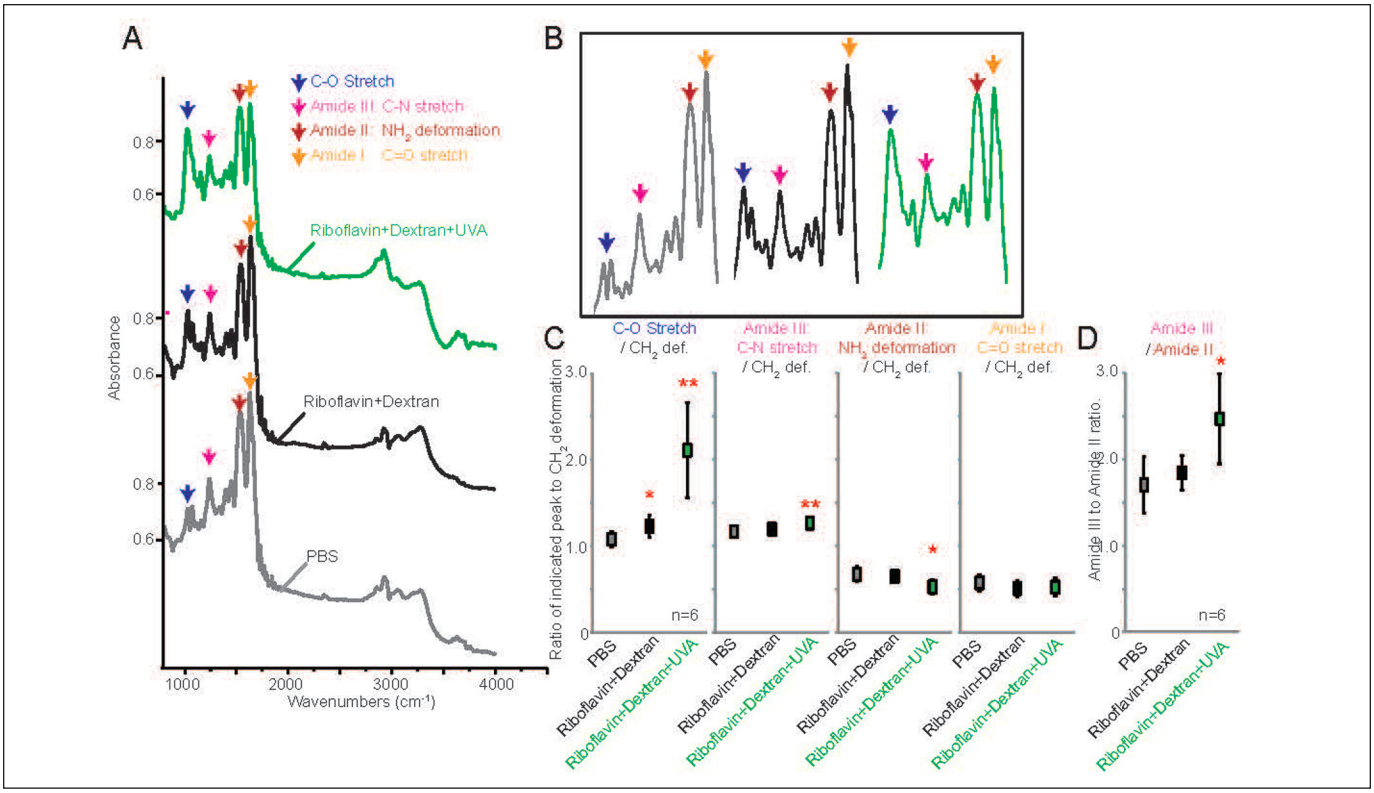

Figure 4. Absorption Fourier transform infrared (FTIR) spectra of porcine corneas following corneal cross-linking treatments. (A) Representative FTIR spectra of corneas treated with phosphate-buffered saline (PBS) (bottom, gray), riboflavin+dextran (middle, black), or riboflavin+dextran+ultraviolet-A (UVA) (top, green). (B) Regions where the characteristic bands are located shown at higher magnification and regions of interest indicated amide I (1,680 to 1,630 cm^{-1}), amide II (1,570 to 1, 515 cm^{-1}), amide III (1,350 to 1,200 cm^{-1}), and CO absorption band (1,150 to 1,000 cm^{-1}). (C) Relative intensity ratio of each characteristic band and (D) conversion rate of amide II to amide III.

ever, we did observe an increase in C-O stretching force in the riboflavin in the dextran-treated corneas compared with controls, indicating that dextran does itself induce collagen changes. A potential explanation for these new bonds is that the dextran-induced dehydration increases the swelling pressure of tissue and therefore the resistance pressure of proteoglycan matrix,[26,27] giving rise to intermolecular forces. These dextran and dehydration effects could help explain some of the apparently contradictory reports in the literature.[5,6,10,11] Interestingly, tissue hydration states have been reported to affect the efficacy of CXL treatment[27]; therefore, hydration states and the osmolarity of the riboflavin solutions could be important factors to consider in protocol modifications.

Our FTIR data revealed significant changes in C-O stretching force and conversion rate of amide bonds following the full Dresden protocol. Lysine-based cross-links following UVA/riboflavin CXL have previously been postulated but not been found chemically,[3,28] and it has been proposed that cross-links form through endogenous carbonyl groups including imidazole formation.[29] Our data support a model where the increased swelling pressure and the involvement of endogenous carbonyls (allysine) leads to the new bond formation.[22] This leads to a broader mechanism where UVA/riboflavin–induced intrafibril bonds present as thickened collagen fibrils and less dense overall structure and drive the increased tissue mechanical strength and resistance to dehydration (**Figure E**, available in the online version of this article).

However, it should be noted that the ultrastructural changes we measured do not fully account for the mechanical effects, suggesting that collagen fibril diameter and spacing are not the only aspects of stromal biology affected by UVA/riboflavin CXL. Effects on other stromal proteins and particularly the interactions of collagen with proteoglycans could be contributing to the stiffening. Proteoglycans within the corneal stroma have been proposed to play a pivotal role in regulating the fibril-fibril spacing and hydration-dehydration properties,[30] but the dehydration-induced decrease in interfibril spacing has prevented us from being able to determine the sole effect of CXL on proteoglycans within our experimental system.

Understanding the stabilization mechanism of UVA/riboflavin CXL is clinically relevant when evaluating modifications to the Dresden protocol and developing

optimal protocols or new keratoconus treatments. This study establishes the standards in terms of mechanical, chemical, and structure/biological changes induced by the Dresden protocol and therefore provides the baseline against which modifications can be judged.

AUTHOR CONTRIBUTIONS

Study concept and design (S-HC, CEW, KJH, AElsheikh); data collection (S-HC, AEliasy, K-JC, Y-RJ, T-HY, T-JW); analysis and interpretation of data (S-HC, AEliasy, K-JC, T-HY, CEW, KJH, AElsheikh); writing the manuscript (S-HC, AEliasy, K-JC, Y-RJ, T-HY, T-JW, CEW, KJH, AElsheikh); critical revision of the manuscript (S-HC, AEliasy, CEW, KJH, AElsheikh); statistical expertise (S-HC, AEliasy, K-JC, T-HY); administrative, technical, or material support (AEliasy, T-JW); supervision (CEW, KJH, AElsheikh)

REFERENCES

1. Andreassen TT, Simonsen AH, Oxlund H. Biomechanical properties of keratoconus and normal corneas. *Exp Eye Res.* 1980;31:435-441.
2. Wollensak G. Crosslinking treatment of progressive keratoconus: new hope. *Curr Opin Ophthalmol.* 2006;17:356-360.
3. Wollensak G, Spoerl E, Seiler T. Riboflavin/ultraviolet-a-induced collagen crosslinking for the treatment of keratoconus. *Am J Ophthalmol.* 2003;135:620-627.
4. Brummer G, Littlechild S, McCall S, Zhang Y, Conrad GW. The role of nonenzymatic glycation and carbonyls in collagen crosslinking for the treatment of keratoconus. *Invest Ophthalmol Vis Sci.* 2011;52:6363-6369.
5. Hayes S, Kamma-Lorger CS, Boote C, et al. The effect of riboflavin/UVA collagen cross-linking therapy on the structure and hydrodynamic behaviour of the ungulate and rabbit corneal stroma. *PloS One.* 2013;8:e52860.
6. Akhtar S, Almubrad T, Paladini I, Mencucci R. Keratoconus corneal architecture after riboflavin/ultraviolet A cross-linking: ultrastructural studies. *Mol Vis.* 2013;19:1526-1537.
7. Spoerl E, Wollensak G, Dittert DD, Seiler T. Thermomechanical behavior of collagen-cross-linked porcine cornea. *Ophthalmologica.* 2004;218:136-140.
8. Spoerl E, Wollensak G, Seiler T. Increased resistance of crosslinked cornea against enzymatic digestion. *Curr Eye Res.* 2004;29:35-40.
9. Wollensak G, Wilsch M, Spoerl E, Seiler T. Collagen fiber diameter in the rabbit cornea after collagen crosslinking by riboflavin/UVA. *Cornea.* 2004;23:503-507.
10. Wang X, Huang Y, Jastaneiah S, et al. Protective effects of soluble collagen during ultraviolet-A crosslinking on enzyme-mediated corneal ectatic models. *PloS One.* 2015;10:e0136999.
11. Wollensak G, Aurich H, Pham DT, Wirbelauer C. Hydration behavior of porcine cornea crosslinked with riboflavin and ultraviolet A. *J Cataract Refract Surg.* 2007;33:516-521.
12. Boote C, Dennis S, Newton RH, Puri H, Meek KM. Collagen fibrils appear more closely packed in the prepupillary cornea: optical and biomechanical implications. *Invest Ophthalmol Vis Sci.* 2003;44:2941-2948.
13. Depalle B, Qin Z, Shefelbine SJ, Buehler MJ. Influence of cross-link structure, density and mechanical properties in the mesoscale deformation mechanisms of collagen fibrils. *J Mech Behav Biomed Mater.* 2015;52:1-13.
14. Whitford C, Studer H, Boote C, Meek KM, Elsheikh A. Biomechanical model of the human cornea: considering shear stiffness and regional variation of collagen anisotropy and density. *J Mech Behav Biomed Mater.* 2015;42:76-87.
15. Raiskup F, Spoerl E. Corneal crosslinking with riboflavin and ultraviolet A: I. Principles. *Ocul Surf.* 2013;11:65-74.
16. Schumacher S, Mrochen M, Wernli J, Bueeler M, Seiler T. Optimization model for UV-riboflavin corneal cross-linking. *Invest Ophthalmol Vis Sci.* 2012;53:762-769.
17. Kohlhaas M, Spoerl E, Schilde T, Unger G, Wittig C, Pillunat LE. Biomechanical evidence of the distribution of cross-links in corneas treated with riboflavin and ultraviolet A light. *J Cataract Refract Surg.* 2006;32:279-283.
18. Seifert J, Hammer CM, Rheinlaender J, et al. Distribution of Young's modulus in porcine corneas after riboflavin/UVA-induced collagen cross-linking as measured by atomic force microscopy. *PloS One.* 2014;9:e88186.
19. Choi S, Lee S-C, Lee H-J, et al. Structural response of human corneal and scleral tissues to collagen cross-linking treatment with riboflavin and ultraviolet A light. *Lasers Med Sci.* 2013;28:1289-1296.
20. Randleman JB, Santhiago MR, Kymionis GD, Hafezi F. Corneal cross-linking (CXL): standardizing terminology and protocol nomenclature. *J Refract Surg.* 2017;33:727-729.
21. Elsheikh A, Wang D, Brown M, Rama P, Campanelli M, Pye D. Assessment of corneal biomechanical properties and their variation with age. *Curr Eye Res.* 2007;32:11-19.
22. Boyce B, Jones R, Nguyen T, Grazier J. Stress-controlled viscoelastic tensile response of bovine cornea. *J Biomech.* 2007;40:2367-2376.
23. Wollensak G, Spoerl E, Seiler T. Stress-strain measurements of human and porcine corneas after riboflavin–ultraviolet-A-induced cross-linking. *J Cataract Refract Surg.* 2003;29:1780-1785.
24. Atherton TJ, Kerbyson DJ. Size invariant circle detection. *Image Vis Comput.* 1999;17:795-803.
25. Yuen H, Princen J, Illingworth J, Kittler J. Comparative study of Hough transform methods for circle finding. *Image Vis Comput.* 1990;8:71-77.
26. Hatami-Marbini H, Etebu E, Rahimi A. Swelling pressure and hydration behavior of porcine corneal stroma. *Curr Eye Res.* 2013;38:1124-1132.
27. Hodson SA. Corneal stromal swelling. *Prog Retin Eye Res.* 1997;16:99-116.
28. Spoerl E, Huhle M, Seiler T. Induction of cross-links in corneal tissue. *Exp Eye Res.* 1998;66:97-103.
29. McCall AS, Kraft S, Edelhauser HF, et al. Mechanisms of corneal tissue cross-linking in response to treatment with topical riboflavin and long-wavelength ultraviolet radiation (UVA). *Invest Ophthalmol Vis Sci.* 2010;51:129-138.
30. Hahn RA, Birk DE. Beta-D xyloside alters dermatan sulfate proteoglycan synthesis and the organization of the developing avian corneal stroma. *Development.* 1992;115:383-393.

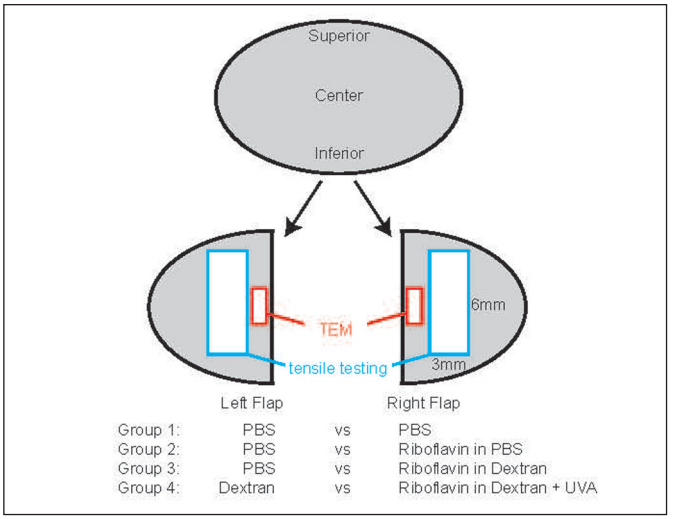

Figure A. Experimental scheme. Each cornea was cut into two segments in a superior-inferior fashion. The right-hand segment was used as an experimental segment, whereas the left-hand segment was used as its corresponding control. After each treatment, specimens were dissected and processed for tensile testing (green hollow rectangle) and transmission electron microscopy (TEM) (red hollow rectangle). S = superior; I = inferior; PBS = phosphate-buffered saline; UVA = ultraviolet-A

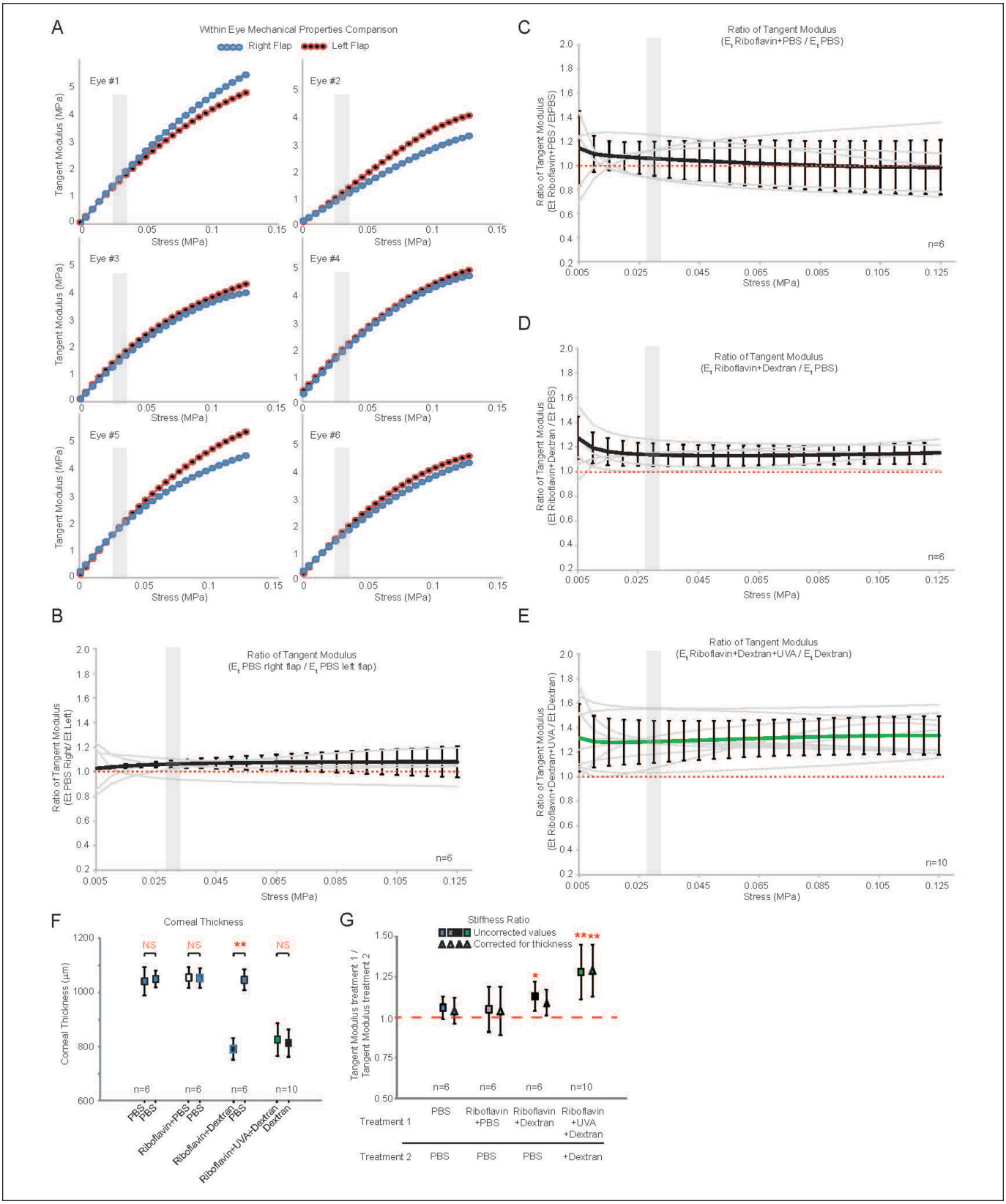

Figure B. The tangent modulus (Et) versus stress (σ) behavior and ratio of tangent modulus of paired samples. (A) The tangent modulus vs stress behavior of right-hand corneal flaps vs left-hand flaps from 6 corneas are plotted. Both flaps were identically treated by soaking in phosphate-buffered saline (PBS). The ratio of tangent modulus between (B) PBS vs PBS (n = 6), (C) riboflavin+PBS vs PBS (n = 6), (D) riboflavin+dextran vs PBS (n = 6), and (E) riboflavin+dextran+ultraviolet-A (UVA) vs dextran only (n = 10). Values from each individual cornea pair tested are indicated by gray lines. Average stiffening ratio ± standard deviation indicated by the bold line and error bars. The red dashed line represented the value of 1 (ie, no difference between paired samples). Gray shaded region in A-E plots represents 0.03 MPa. (F) Average thickness measurement of each comparison group after treatment. (G) The stiffening ratio at 0.03 MPa with and without correction for tissue thickness changes. Values in F and G denote mean ± standard deviation (SD). *$P < .05$. **$P < .01$. NS = not significant

TABLE A

Average Thickness and Stiffening Ratio at 0.03 MPa of Each Group Before and After Thickness Correction[a]

Right Flap/Left Flap	No. of Samples	Average Thickness (μm)	Average Stiffening Ratio at 0.03 MPa Stress[b]	
			Before Thickness Correction	After Thickness Correction
$Et_{experimental\ PBS}/Et_{control\ PBS}$	6	1,042 ± 52/1,050 ± 31	1.06 ± 0.07	1.04 ± 0.08
$Et_{riboflavin+PBS}/Et_{PBS}$	6	1,056 ± 38/1,053 ± 37	1.05 ± 0.14	1.04 ± 0.15
$Et_{riboflavin+dextran}/Et_{PBS}$	6	791 ± 40/1,047 ± 39	1.13 ± 0.09[b]	1.09 ± 0.08
$Et_{riboflavin+dextran+UVA}/Et_{dextran}$	10	826 ± 60/813 ± 51	1.28 ± 0.17[b]	1.29 ± 0.16[b]

[a] *Values are presented as mean ± standard deviation.*
[b] $P < .05$ *compared with its control.*

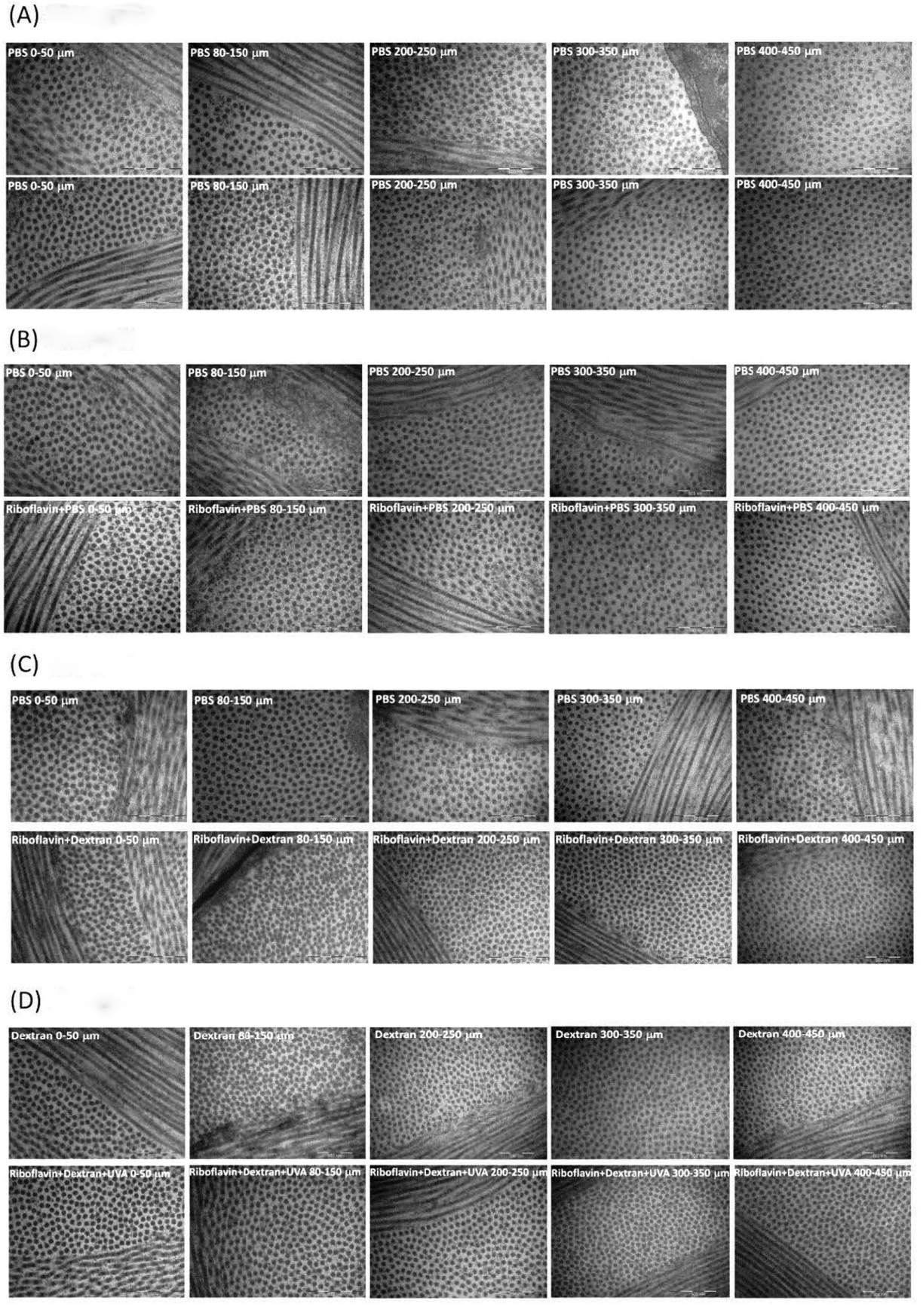

Figure C. Transmission electron microscopy (TEM) images of porcine corneas imaged at different depth intervals following phosphate-buffered saline (PBS), dextran, and/or UVA/riboflavin treatment. Representative TEM images of (A) PBS, (B) riboflavin+PBS , (C) riboflavin+dextran, or (D) riboflavin+dextran+UVA and their corresponding controls at five depth intervals of 0 to 50, 80 to 150, 200 to 250, 300 to 350, and 400 to 450 μm.

TABLE B

Mean Diameter, Interfibrillar Spacing, and Density of Collagen Fibrils of Corneal Segments at Different Depth Intervals[a,b]

Group	No. of Samples	Depth Range (mm)	Mean Diameter of Collagen (nm)	Interfibrillar Spacing (nm)	Density of Collagen (N/900 nm^2)
PBS vs PBS	6	0 to 50	39.64 ± 1.13 vs 38.69 ± 1.54	29.84 ± 2.12 vs 30.25 ± 0.70	18.98 ± 1.56 vs 19.56 ± 1.37
		80 to 150	37.25 ± 1.10 vs 36.41 ± 1.42	30.52 ± 1.64 vs 30.78 ± 0.69	18.36 ± 1.17 vs 19.25 ± 2.00
		200 to 250	35.31 ± 1.15 vs 34.84 ± 1.16	31.32 ± 1.71 vs 30.03 ± 1.17	20.13 ± 1.56 vs 20.47 ± 1.81
		300 to 350	32.02 ± 1.08 vs 32.02 ± 1.32	32.03 ± 1.49 vs 31.31 ± 1.11	19.99 ± 2.08 vs 19.93 ± 1.46
		400 to 450	30.68 ± 0.89 vs 30.27 ± 1.17	32.38 ± 1.26 vs 31/52 ± 1.34	20.22 ± 2.59 vs 19.55 ± 2.08
PBS vs riboflavin+PBS	6	0 to 50	38.63 ± 1.34 vs 38.83 ± 1.11	30.24 ± 0.63 vs 30.55 ± 0.94	19.70 ± 1.54 vs 19.90 ± 1.04
		80 to 150	35.61 ± 1.38 vs 35.95 ± 0.66	30.75 ± 0.59 vs 31.22 ± 1.48	19.47 ± 1.86 vs 19.18 ± 2.00
		200 to 250	34.34 ± 1.63 vs 34.32 ± 1.15	30.65 ± 1.65 vs 30.39 ± 0.98	20.06 ± 0.81 vs 19.18 ± 2.00
		300 to 350	31.18 ± 1.45 vs 30.99 ± 0.92	31.38 ± 1.29 vs 32.30 ± 0.76	21.42 ± 0.76 vs 20.91 ± 1.19
		400 to 450	30.28 ± 0.98 vs 30.23 ± 0.52	31.10 ± 0.97 vs 31.95 vs 1.70	21.17 ± 1.18 vs 20.82 ± 1.48
PBS vs riboflavin+dextran	6	0 to 50	38.78 ± 1.68 vs 34.68 ± 0.63**	30.83 ± 1.35 vs 21.68 ± 2.20**	20.82 ± 1.23 vs 28.42 ± 1.03**
		80 to 150	36.02 ± 1.52 vs 31.85 ± 0.97**	30.77 ± 1.13 vs 21.59 ± 1.34**	18.82 ± 1.96 vs 27.14 ± 1.82**
		200 to 250	34.51 ± 1.11 vs 30.36 ± 1.63**	30.49 ± 0.94 vs 22.93 ± 1.69**	19.21 ± 1.42 vs 28.20 ± 1.39**
		300 to 350	31.11 ± 1.20 vs 29.83 ± 0.86*	31.10 ± 0.92 vs 23.41 ± 0.96	20.11 ± 1.24 vs 26.40 ± 1.79
		400 to 450	30.62 ± 1.92 vs 29.45 ± 0.52	31.19 ± 1.21 vs 23.95 ± 0.68**	20.15 ± 0.93 vs 27.07 ± 1.17**
Dextran vs riboflavin+ dextran+UVA	10	0 to 50	35.85 ± 1.70 vs 36.75 ± 1.03	20.53 ± 1.83 vs 22.43 ± 3.49	20.03 ± 1.74 vs 26.31 ± 1.42*
		80 to 150	32.74 ± 1.39 vs 34.32 ± 1.23**	21.93 ± 2.95 vs 28.44 ± 2.95	28.44 ± 1.32 vs 25.46 ± 1.71**
		200 to 250	30.75 ± 1.05 vs 32.50 ± 1.19**	22.52 ± 1.97 vs 23.37 ± 2.71	28.34 ± 1.41 vs 25.24 ± 1.61
		300 to 350	30.47 ± 1.36 vs 30.46 ± 1.42	23.23 ± 1.81 vs 22.11 ± 1.32	26.69 ± 1.94 vs 27.03 ± 1.78
		400 to 450	30.38 ± 1.17 vs 30.21 ± 0.80	23.75 ± 1.68 vs 22.89 ± 2.21	26.79 ± 1.77 vs 27.34 ± 1.82

PBS = phosphate-buffered saline; UVA = unltraviolet-A

[a]*Values are presented as mean ± standard deviation.*

[b]*P < .05 is indicated by an asterisk compared with its control. ** indicates increase compared with control, * represents decrease compared with control.*

TABLE C

Area Ratio Corresponding to Indicated Characteristic Bands in FTIR Spectra[a,b]

Ratio	PBS	Riboflavin+Dextran	Riboflavin+Dextran+UVA
No. of samples	6	6	6
C-O stretch/-(CH_2)-deformation	1.08 ± 0.09	1.23 ± 0.12*	2.10 ± 0.55**
Amide II/-(CH_2)-deformation	0.67 ± 0.08	0.64 ± 0.06	0.52 ± 0.08*
Amide III/-(CH_2)-deformation	1.16 ± 0.02	1.19 ± 0.02	1.26 ± 0.04**
Amide I/-(CH_2)-deformation	0.57 ± 0.09	0.50 ± 0.09	0.52 ± 0.10
Amide III/amide I	1.70 ± 0.33	1.84 ± 0.20	2.47 ± 0.51*

FITR = Fourier transform infrared spectroscopy; PBS = phosphate-buffered saline; UVA = ultraviolet-A

[a]*Values are presented as mean ± standard deviation.*

[b]*P < .05 is indicated by an asterisk compared with its control. ** indicates increase compared with control, * represents decrease compared with control.*

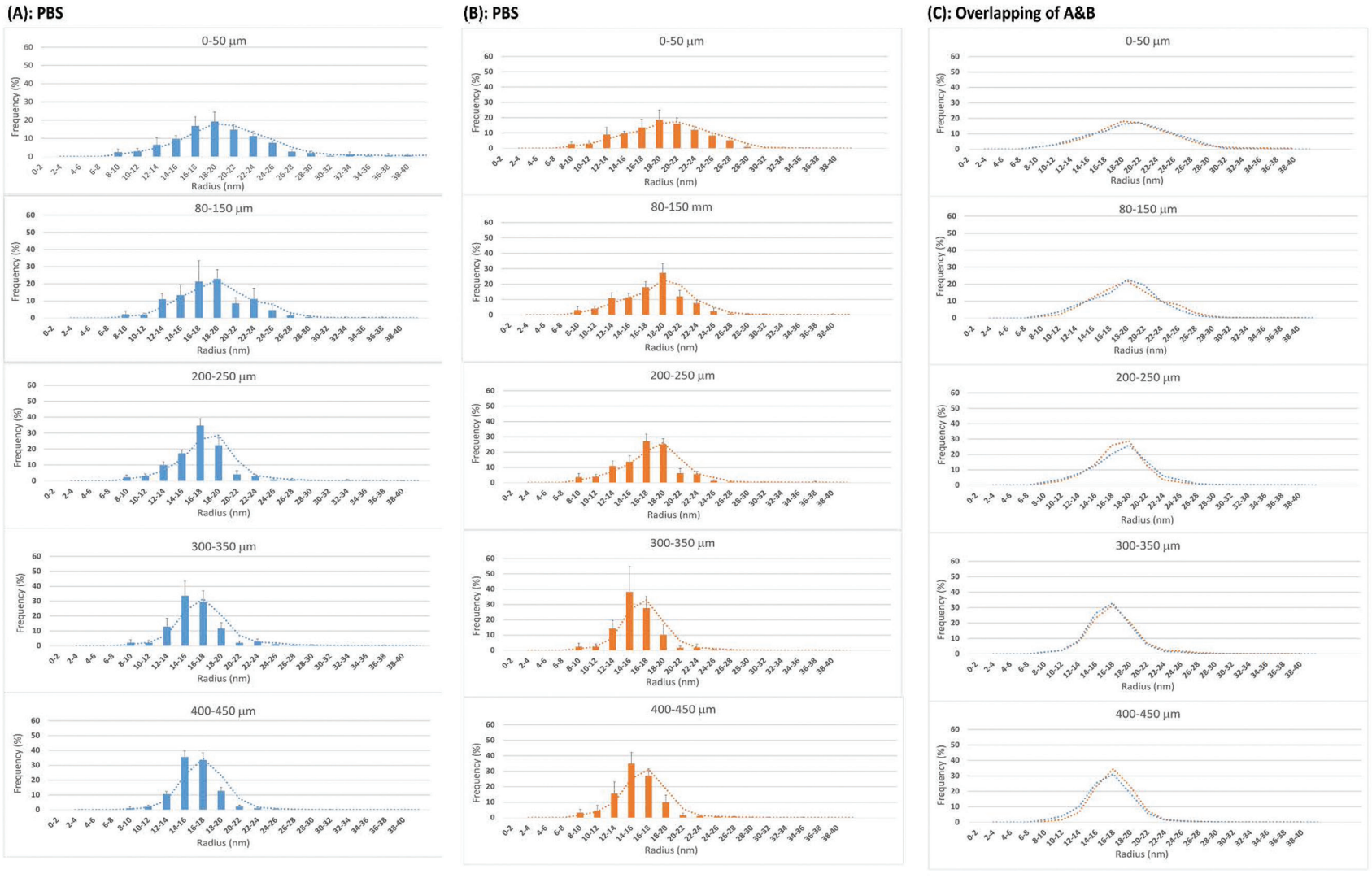

Figure D. Collagen radius distribution of each treatment group at each depth interval. The distribution of control segments (blue): (A) phosphate-buffered saline (PBS), (D) PBS, (G) PBS, and (K) dextran, and the experimental segments (orange): (B) PBS, (E) riboflavin+PBS, (H) riboflavin+dextran, and (L) riboflavin+dextran+UVA. Dashed lines represent trend curves. The overlapped curves (C, F, I, J, M) were used for detecting the shifting of distribution in radius between control and experimental segments. The data were obtained at five depth intervals of 0 to 50, 80 to 150, 200 to 250, 300 to 350, and 400 to 450 μm. A *P* value of less than .05 is indicated by an asterisk compared with its internal control.

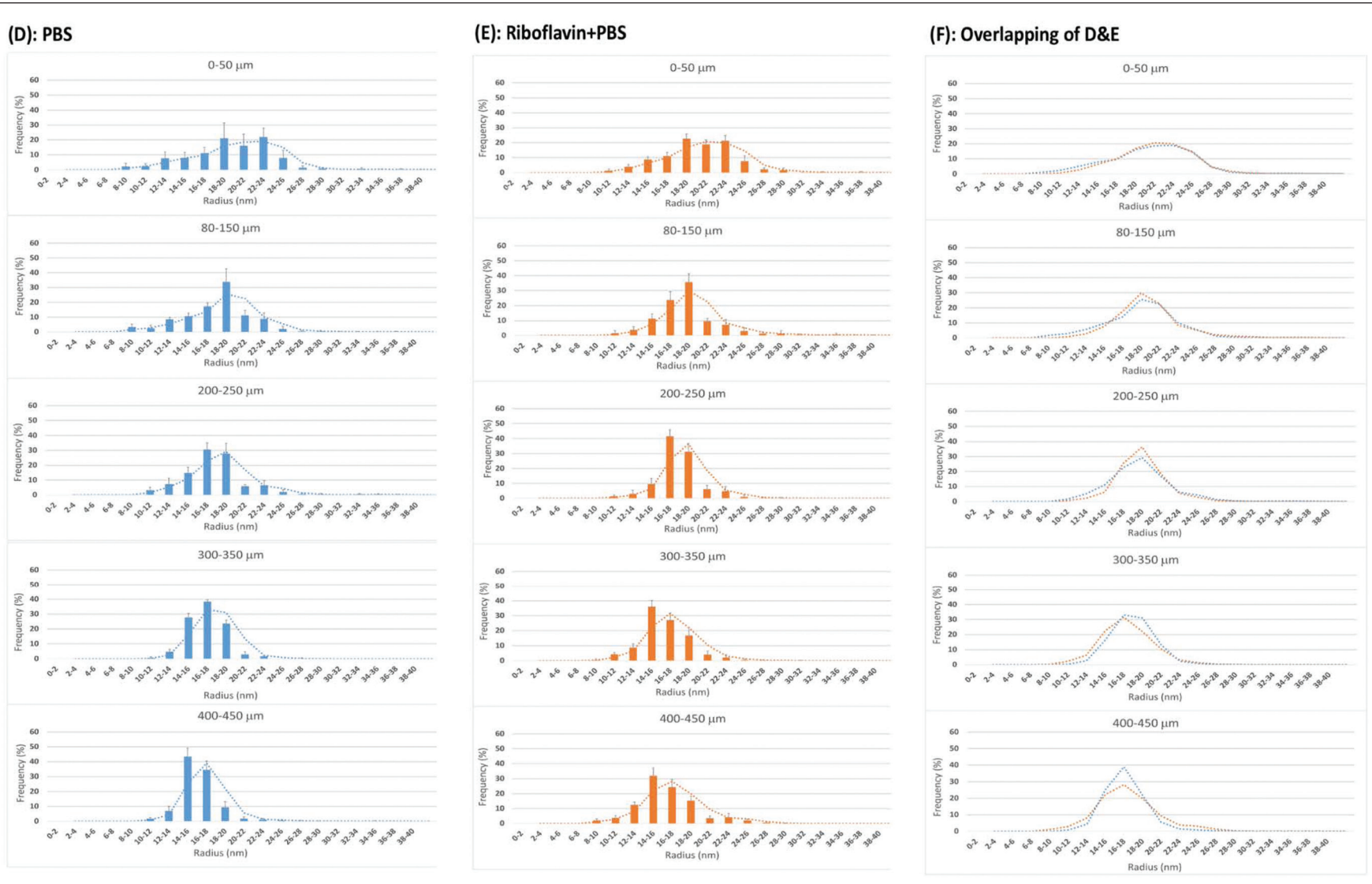

Figure D (cont'd). Collagen radius distribution of each treatment group at each depth intervl. The distribution of control segments (blue): (A) phosphate-buffered saline (PBS), (D) PBS, (G) PBS, and (K) dextran, and the experimental segments (orange): (B) PBS, (E) riboflavin+PBS, (H) riboflavin+dextran, and (L) riboflavin+dextran+UVA. Dashed lines represent trend curves. The overlapped curves (C, F, I, J, M) were used for detecting the shifting of distribution in radius between control and experimental segments. The data were obtained at five depth intervals of 0 to 50, 80 to 150, 200 to 250, 300 to 350, and 400 to 450 μm. A *P* value of less than .05 is indicated by an asterisk compared with its internal control.

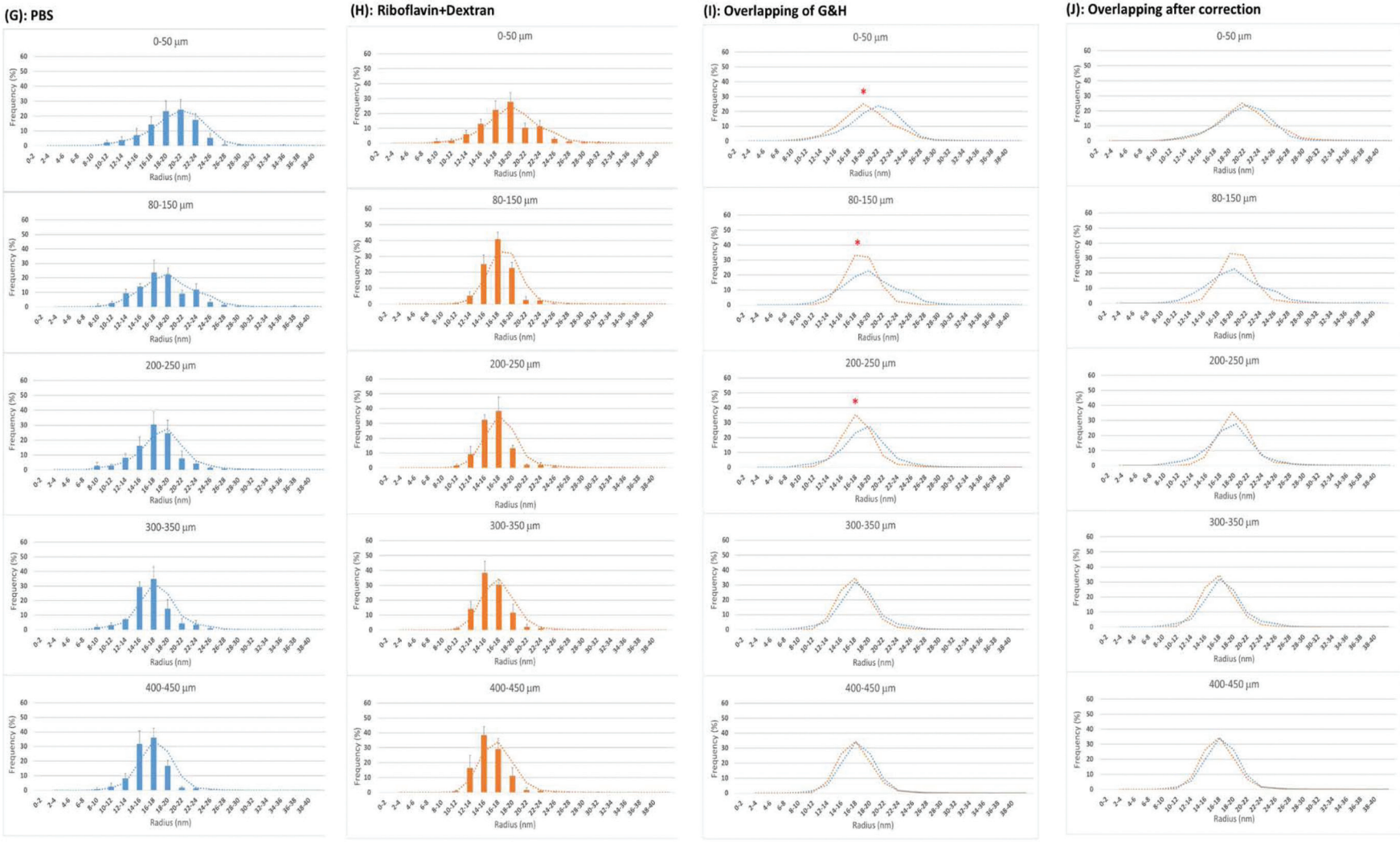

Figure D (cont'd). Collagen radius distribution of each treatment group at each depth interval. The distribution of control segments (blue): (A) phosphate-buffered saline (PBS), (D) PBS, (G) PBS, and (K) dextran, and the experimental segments (orange): (B) PBS, (E) riboflavin+PBS, (H) riboflavin+dextran, and (L) riboflavin+dextran+UVA. Dashed lines represent trend curves. The overlapped curves (C, F, I, J, M) were used for detecting the shifting of distribution in radius between control and experimental segments. The data were obtained at five depth intervals of 0 to 50, 80 to 150, 200 to 250, 300 to 350, and 400 to 450 μm. A *P* value of less than .05 is indicated by an asterisk compared with its internal control.

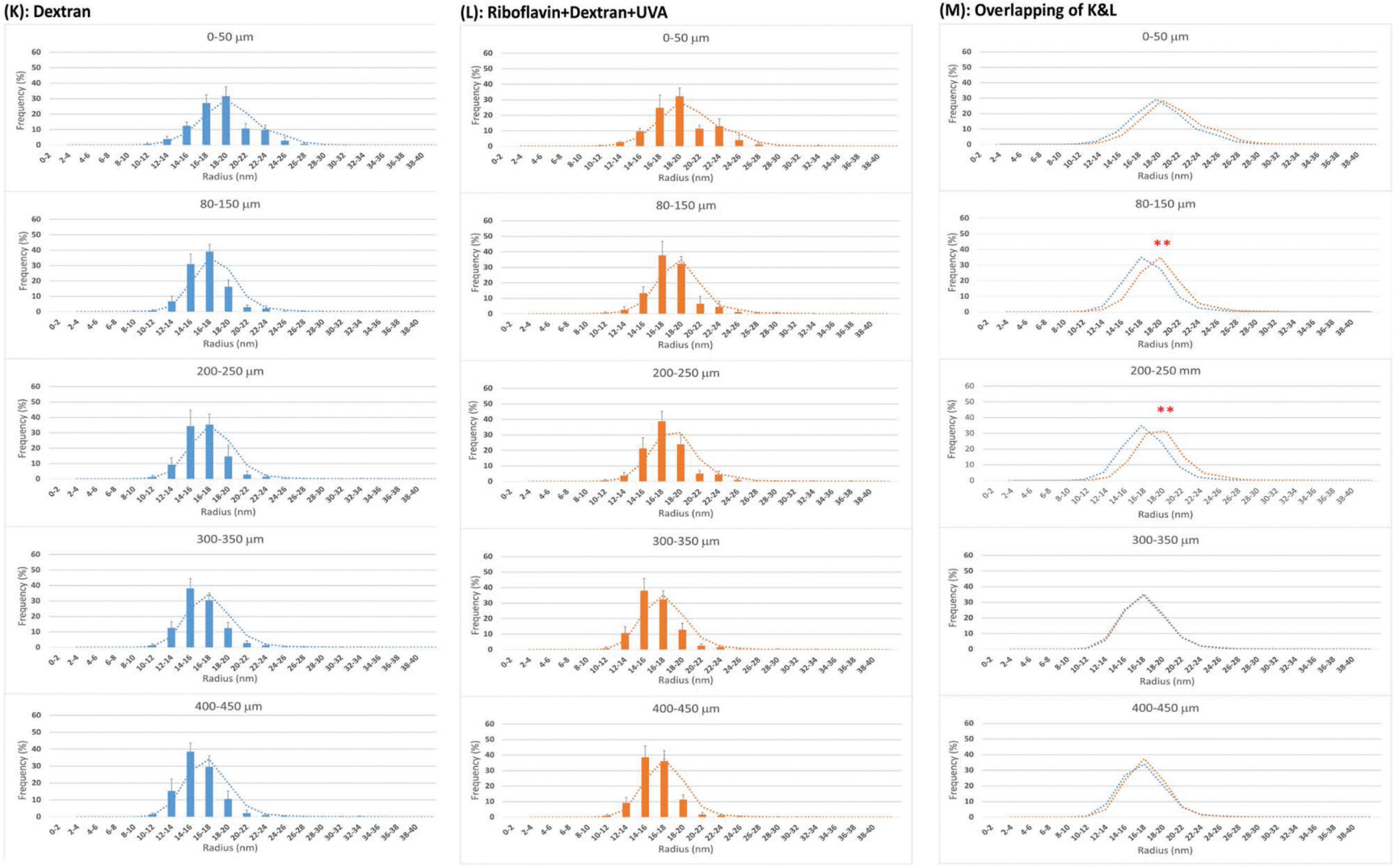

Figure D (cont'd). Collagen radius distribution of each treatment group at each depth interval. The distribution of control segments (blue): (A) phosphate-buffered saline (PBS), (D) PBS, (G) PBS, and (K) dextran, and the experimental segments (orange): (B) PBS, (E) riboflavin+PBS, (H) riboflavin+dextran, and (L) riboflavin+dextran+UVA. Dashed lines represent trend curves. The overlapped curves (C, F, I, J, M) were used for detecting the shifting of distribution in radius between control and experimental segments. The data were obtained at five depth intervals of 0 to 50, 80 to 150, 200 to 250, 300 to 350, and 400 to 450 μm. A *P* value of less than0.05 is indicated by an asterisk compared with its internal control.

TABLE D

Parameters Used in Correction of the Collagen Fibril Radius Distribution Curves

	Depth (μm)				
Correction Parameter	**0 to 50**	**80 to 150**	**200 to 250**	**300 to 350**	**400 to 450**
Decreased % of collagen diameter	10.41%	12.83%	14.12%	4.18%	3.01%
Decreased % of interfibrillar spacing	29.03%	28.06%	27.39%	27.70%	26.91%
Decreased % of collagen diameter on overall loss	26.39%	31.01%	34.02%	13.11%	10.06%
Decreased % of interfibrillar spacing on overall loss	73.61%	68.99%	65.98%	86.89%	89.94%
Hydration loss % of collagen diameter	4.46%	5.24%	5.75%	2.21%	1.70%
Hydration loss % of interfibrillar spacing	12.45%	11.67%	11.16%	14.70%	15.21%
Remaining hydration % of collagen diameter	95.54%	94.76%	94.25%	97.79%	98.30%
Remaining hydration % of interfibrillar spacing	87.55%	88.33%	88.84%	85.30%	84.79%
Swelling factor for correction of distribution of collagen diameter	1.05	1.06	1.06	1.02	1.02

Overall tissue dehydration % = 16.91% (1.047 mm thickness/ 5.01; 0.791 mm/ 4.16).
*Thickness–hydration (T-H) relationship of porcine cornea: T = 0.2*e^(0.33*H).*
Swelling factor: 1 / Remaining tissue hydration

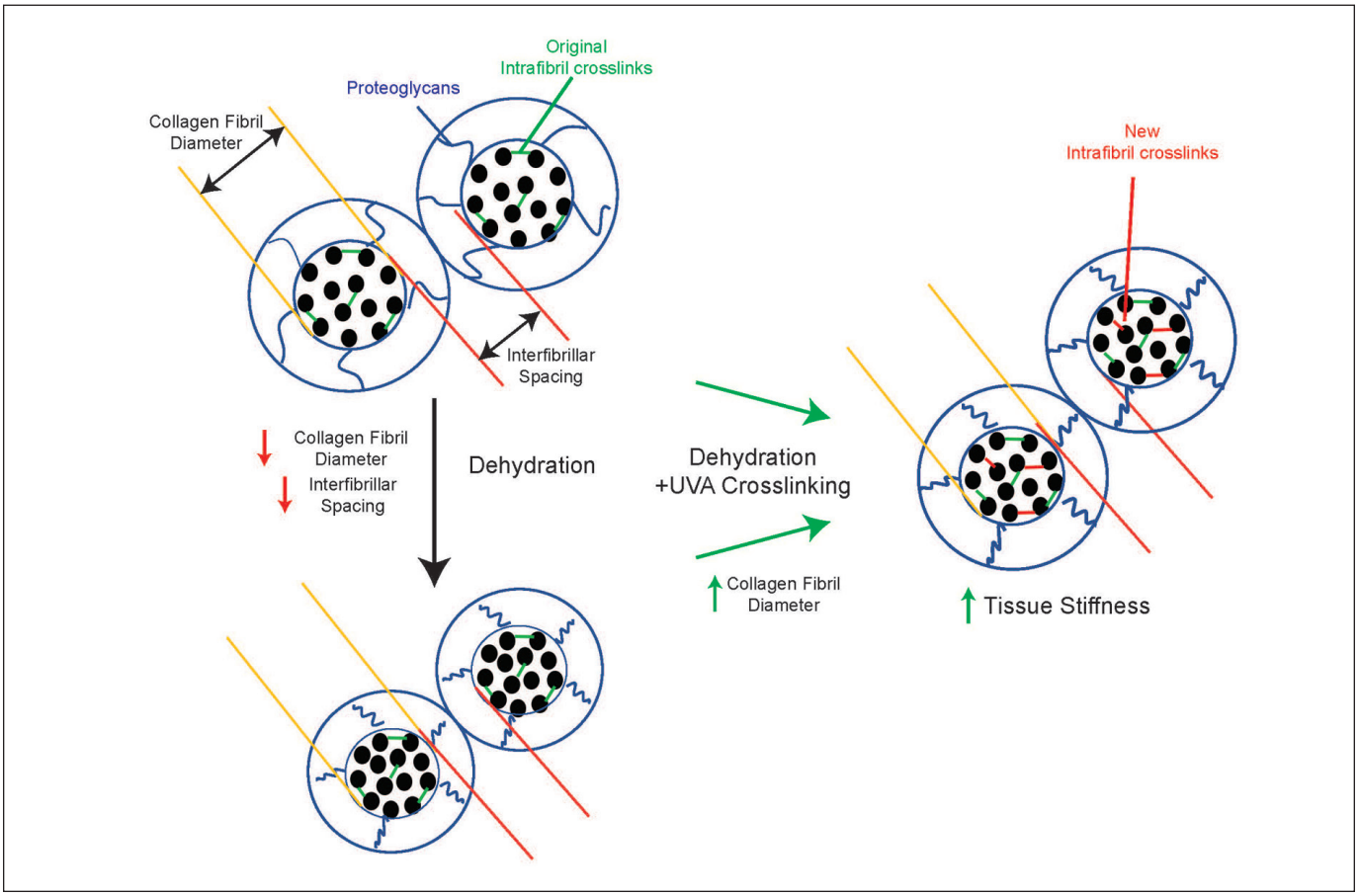

Figure E. Proposed model of ultraviolet-A (UVA)/riboflavin corneal cross-linking with the presence of dextran. The black solid circle, blue solid line, green solid line, and red solid line represent the collagen molecules, proteoglycans, original cross-links formed between collagen molecules, and additional cross-links induced by UVA/riboflavin corneal cross-linking treatment, respectively.